Chapter 4

Experimental results

4.1 Introduction

The HTRI analyses predicted vibration problems at certain mass flow rates. Some additional calculations were also done to determine a number of other important mass flow rates at which vibration may occur (Chapter 2). In Chapter 3, CFD analyses were performed to determine if the velocities used by the HTRI analyses were correct and also to get a better understanding of the flow patterns through the heat exchanger. All the above methods can be used to predict whether or not the shell-and-tube heat exchanger may experience vibration problems at a specific operating mass flow rate. To test whether this predicted vibration actually occurred, vibration measurements on the ES 208 Tail gas shell-and-tube heat exchanger were done at different operational flow rates. Figure 4.1 shows the ES 208 Tail gas heat exchanger at Sasol Synthetic Fuels (SSF).

Figure 4.1 ES 208 Tail gas shell-and-tube heat exchanger

4.2 Measuring procedure

To verify the HTRI and CFD results, it is necessary to do vibration measurements on the heat exchanger. It is not always practical to measure on the inside of the heat exchanger:

- Because of the pressure at which the heat exchanger operates;
- The gas on the shell-side is very corrosive and poisonous; and
- The clearances between the tubes are very small and this makes it inaccessible to vibration equipment.

The vibration measurements were therefore taken on the supports and the shell of the heat exchanger. The operational measurements are covered below, followed by the non-operational measurements.

4.2.1 Operational measurements

The following operational measurements were taken on the ES 208 Tail gas heat exchanger (figure 4.2) at SSF.

- The response of the shell at different flow velocities (positions 1, figure 4.2).
- The response of the supports at different flow velocities (position 2)
- Strain gauge measurements at different flow velocities (position 3).

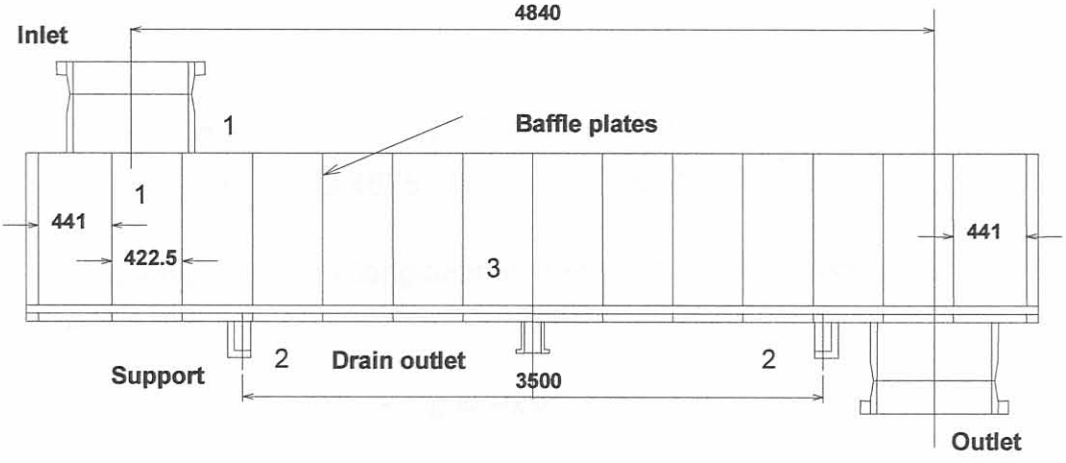

Figure 4.2: Heat exchanger layout

a) Shell and support response measurements

The process of determining tube vibration can be simplified by establishing the relationship between the shell and support vibration and the tube vibration. For this purpose, strain gauges and accelerometers were used. Strain calculations were made to determine the number of strain gauges needed per position to sufficiently measure strain. To obtain the shell bending in the x- and y- directions, at least three strain gauge positions (90 ° apart) are needed, but four positions are preferred, especially if poor contact between the gauge and shell exists.

Strain calculations:

The deflection curve equation (equation 4.1) was obtained using the maximum deflection given by the HTRI results.

$$y = \left(-7.4694 \times 10^{-4}\right)x^2 + \left(9.4675 \times 10^{-4}\right)x \qquad 4.1$$

By differentiating equation 4.1 the angle of rotation of the beam (θ) can be obtained.

$$\theta(x) = \arctan\left(2\left(-7.4694 \times 10^{-4}\right)x + 9.4675 \times 10^{-4}\right) \qquad 4.2$$

The curvature (κ) is the reciprocal of the radius of curvature. For small beam deflections, the distance (*ds*) along the curve may be taken as its horizontal projection (*dx*).

$$\kappa = \frac{d\theta}{dx} = \frac{2\left(-7.4694 \times 10^{-4}\right)}{1 + \left(9.4675 \times 10^{-4} + 2\left(-7.4694 \times 10^{-4}\right)x\right)^2} \qquad 4.3$$

The relationship between longitudinal normal strain and curvature is given by equation 4.4 (Gere and Timoshenko, 1995).

$$\varepsilon = -\kappa y \qquad 4.4$$

where *y* equals the distance between the centre line of the tube and the outside diameter of the tube.

By using equations 4.3 and 4.4, the maximum strain is calculated at 14.2 $\mu\varepsilon$ (micro strain). The strain gauge may be able to measure 14 micro strain but the noise of the associated electronic equipment is in the order of 20 micro strain making accurate measurement with only one strain gauge per position impossible. Four strain gauges were used to amplify the strain measured and were configured as shown in figure 4.3. Two strain gauges in series were connected in parallel to another two strain gauges in series (figure 4.3). This was done to balance the resistance of the Weatstone-bridge.

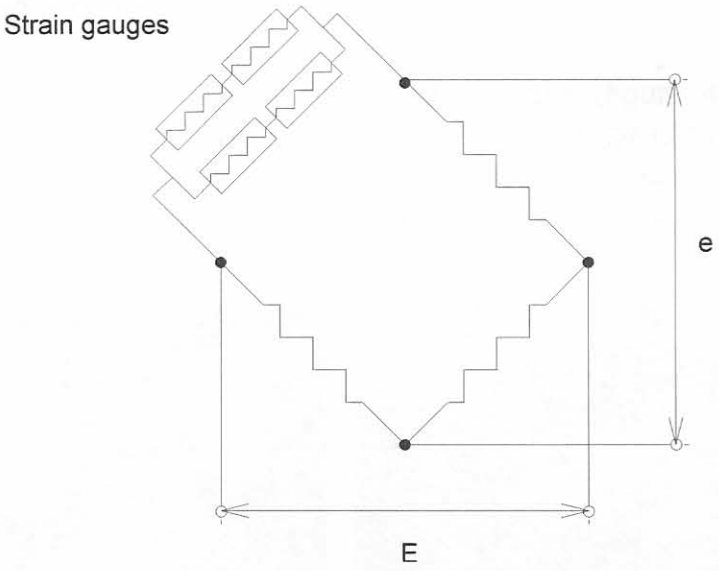

Figure 4.3: Strain gauge configuration

4.2.2 Non-operational measurements

For normal tube-to-baffle clearances, it can be assumed that the tubes are simply supported at the baffle plates, the tolerances of the fitting of the tube may influence the natural frequencies of the tubes. The baffle cut divides some of the tube holes (see figure 2.2), causing those tubes to be supported in one dimension only. Other factors such as corrosion damage, vibration damage and thermal expansion can also influence the natural frequencies.

With non-operational measurements other factors such as external sources of vibration can also be obtained. These include vibration transmitted to the heat exchanger via the foundations and supports of the heat exchanger, as well as the piping connected to the heat exchanger. This is an important part of the measuring procedure, especially if the measurements are taken on a plant where various other sources may cause external vibration.

4.3 Results

Vibration measurements on the heat exchanger were taken on three occasions. In the section that follows, as well as in Appendix E, the results of the vibration measurements will be covered in detail and in Chapter 5 these results will be compared to the predicted values of the HTRI analyses (Chapter 2) as well as the CFD results (Chapter 3).

4.3.1 Shell and support response

Vibration measurements on the shell and supports (figure 4.4) were taken by using three 500 mV/g accelerometers (Entek E326A02), one 100 mV/g accelerometer (Entek E327A01), four 2 V/g accelerometers (PCB 393A11) and 16 KFW-5-120-C1-16L5M2R strain gauges (four at each position).

a) Measuring position at inlet of heat exchanger (A4) (Position 1 from figure 4.2) *b) Measuring position 90° to outlet (A2)*

c) Measuring position at outlet support (B1 & B2) (Position 2 from figure 4.2) *d) Measuring position at inlet support (B3 & B4)*

e) Measuring position at centre of HE *f) Strain gauge measurements (R4)*

Fig. 4.4: Vibration measurement positions

Some of the measuring positions, accelerometers and strain gauges that were used are shown in figure 4.4 (refer to Appendix D for more information on measuring positions).

The flow rate through the heat exchanger was varied by first opening the bypass valve in 100 mm increments. After the bypass valve was fully opened, the heat exchanger inlet valve was closed with 100mm increments (figures 4.5 and 4.6).

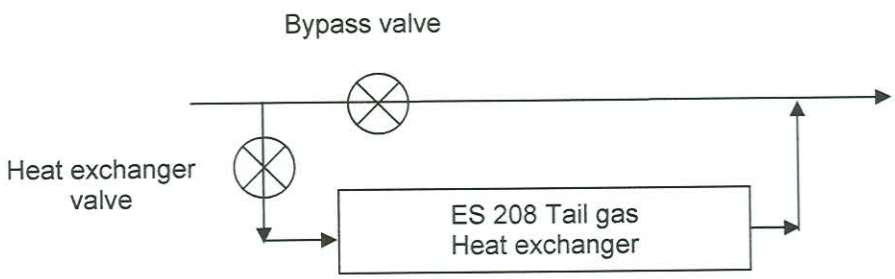

Figure 4.5: Valve configuration

The losses through the two loops were calculated using the pressure drop curve obtained by the HTRI analyses (figure 2.7). (Refer to Appendix B for more detail). The HTRI pressure drop curve was first compared to the CFD pressure drop results through the heat exchanger, as shown in figure 3.11.

The CFD pressure drop was only obtained for lower flow rates because of the limit of y^+ values. The two pressure drop curves compare very well over the flow velocity range and was therefore suitable to be used for the flow rate calculations.

Figure 4.6: 24" Wedge gate valve being closed

The time at which each measurement was taken, was recorded. Logged flow rates at other points in the piping system (upstream) was used to determine the specific flow rate for each measurement. This data was also used for a Power Spectrum Density (PSD) curve, to determine the frequency of pressure fluctuation in the supplied tail gas. The flow rates in normal cubic meters per hour (km^3n/h) are given in figure 4.7 for the two ES 208 Tail gas heat exchangers that are in parallel, as well as the combined flow rate. The PSD curve confirmed randomly fluctuating flow before entering the heat exchanger. The heat exchanger that was used for the measurements is indicated with "B".

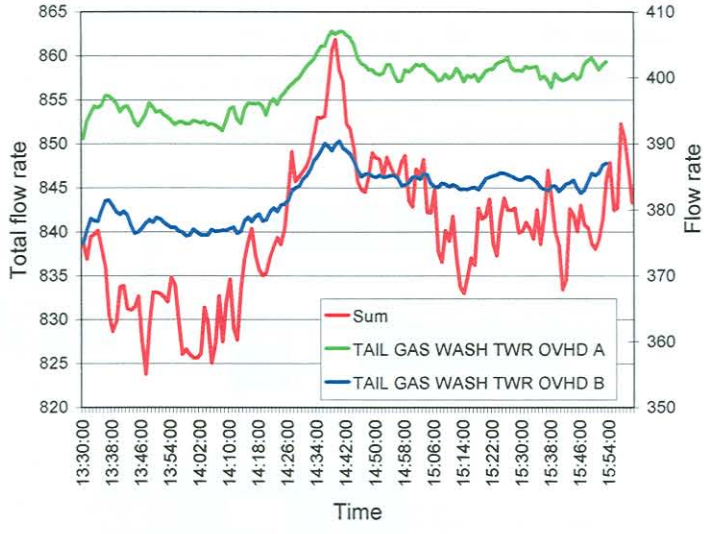

Figure 4.7: Flow rate in km^3n/h for the two tail gas heat exchangers.

The flow rates in figure 4.7 are given at normal temperature and pressure (273 K and 101kPa). The density of the gas at normal temperature and pressure were calculated (Appendix A) and used to convert the volumetric flow rates to mass flow rates. Table 4.1 gives the mass flow rates as calculated in Appendix B. The wedge gate valve average loss coefficients from White (1994) were used to obtain the losses across the valves.

Table 4.1: Mass flow rates through the heat exchanger

Set	Velocity (m/s)	Mass flow rate (kg/s)
1	14.7797	83.42325
2	3.4873	19.68374
3	2.1131	11.92732
4	1.402	7.913393
5	1.1158	6.297841
6	0.9699	5.474317
7	0.9194	5.189442
8	0.8735	4.930306
9	0.7931	4.476549
10	0.6087	3.435545
11	0 (non operational)	0
12	0 (non operational)	0

A record length of 1024 samples was used and twenty averages were taken for every set of measurements. The sampling frequency was 256 Hz and a Hanning window was used. PSDs were calculated for each measurement set, using Siglab 20-42 data acquisitioning equipment. For the strain gauge measurements a KWS 3073 strain gauge amplifier was used (see figure. 4.8).

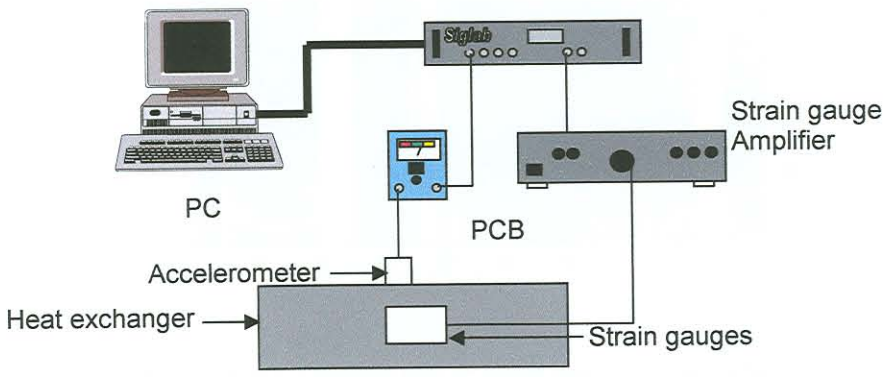

Figure. 4.8: Measuring equipment configuration

Waterfall plots for the strain gauge measurements for the 12 measuring sets are shown in figure 4.9, as well as a contour plot in figure 4.10. From figure 4.10 an increase in strain amplitude at 12.5 Hz, 20 Hz and 28 Hz can be detected. The 28 Hz line coincides with one of the predicted natural frequencies. A slight increase in amplitude is visible at a mass flow rate of 5.5 kg/s (set 6). Above 30 Hz no other frequencies are detected. This may be due to rigid body vibration or small displacement associated with the vibration frequency which results in strain measurements that are smaller than the electronic noise of the equipment. (Appendix E, figures E.1 to E.6)

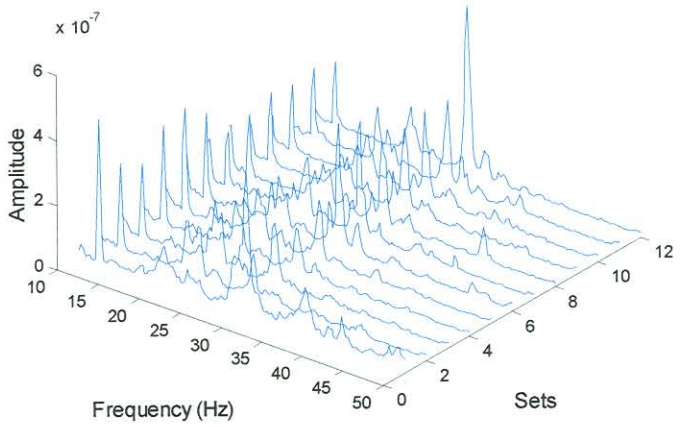

Figure 4.9: Waterfall plot of strain gauge measurements

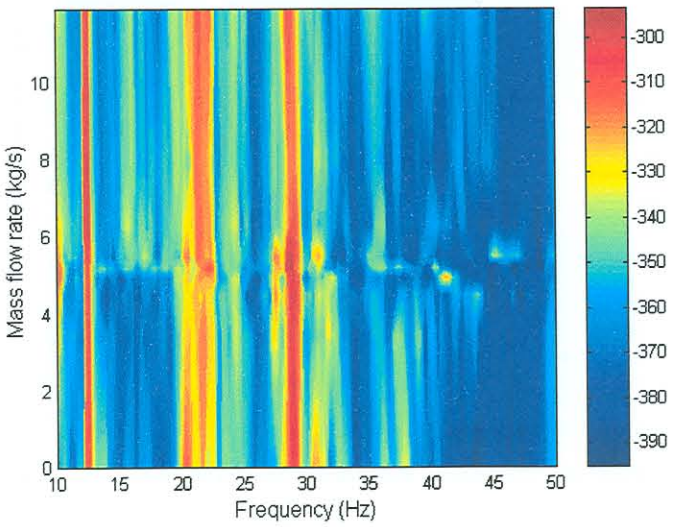

Figure 4.10: Contour plot of strain gauge measurements

The support measurements as shown in figures 4.11 and 4.12, as well as in Appendix E (figures E.7 to E.14), indicated vibration between 27.5 Hz and 28.5 Hz. These values are similar to the HTRI and FEM predicted values of 28.56 Hz and 27.76 Hz respectively. Vibration bands between 35 Hz and 43 Hz, as well as between 53 Hz and 56 Hz were observed. Large vibration amplitudes were also measured at 80 Hz.

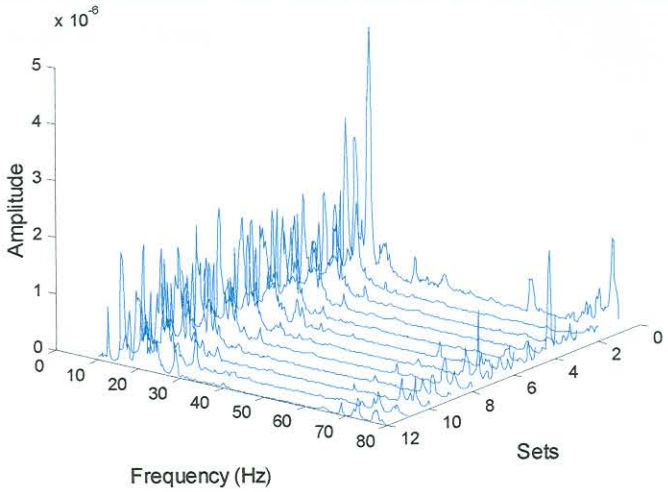

Figure 4.11: Acceleration measurement at support

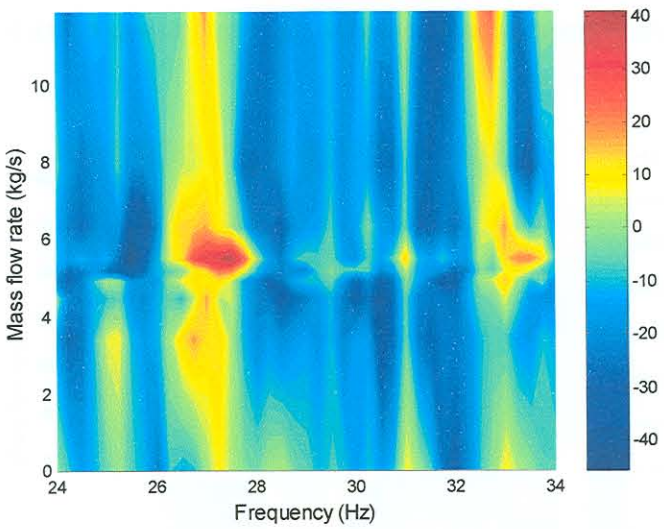

Figure 4.12: Contour plot of difference in support measurements

Measurements at the shell of the heat exchanger indicated vibration throughout the heat exchanger at 24 Hz, 28.5 Hz and 36 Hz (figures 4.13, 4.14 and Appendix E figures E.15 to E.22). Frequency bands between 50 Hz and 60 Hz, and 70 Hz and 80 Hz were also observed.

In both the shell and support measurements an increase in vibration amplitude at a mass flow rate of about 6 kg/s and frequencies of 27.5 Hz of 28.5 Hz, were visible. At some measuring position the amplitude of vibration, at these frequencies, decreased at higher flow rates.

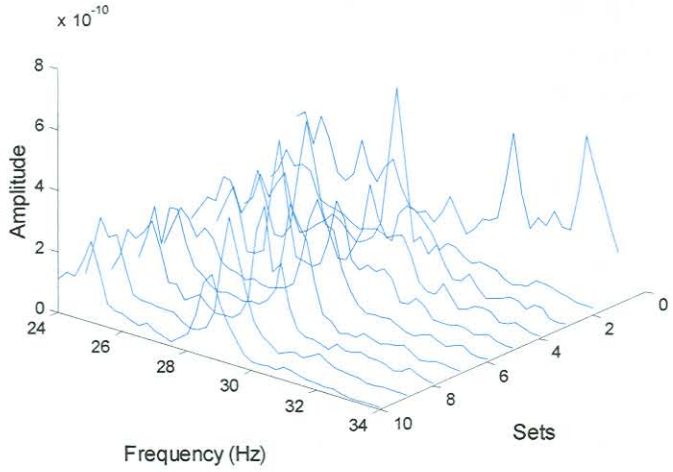

Figure 4.13: Waterfall plot of acceleration measurements at the outlet

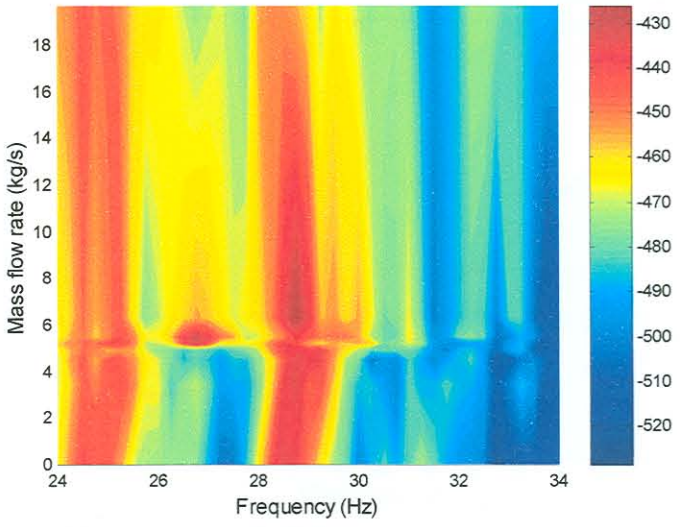

Figure 4.14: Contour plot of acceleration measurements